

See discussions, stats, and author profiles for this publication at: <https://www.researchgate.net/publication/256469829>

Insights into Stabilization of a Viral Protein Cage in Templating Complex Nanoarchitectures: Roles of Disulfide Bonds

ARTICLE in *SMALL* · FEBRUARY 2014

Impact Factor: 8.37 · DOI: 10.1002/smll.201300860 · Source: PubMed

CITATIONS

2

READS

57

8 AUTHORS, INCLUDING:



Feng Li

Wuhan Institute Of Virology

18 PUBLICATIONS 577 CITATIONS

[SEE PROFILE](#)



Kun Zhou

Suzhou Institute of Nano-Tech and Nano-Bi...

4 PUBLICATIONS 51 CITATIONS

[SEE PROFILE](#)

Insights into Stabilization of a Viral Protein Cage in Templating Complex Nanoarchitectures: Roles of Disulfide Bonds

Feng Li, Huiling Chen, Lingzhi Ma, Kun Zhou, Zhi-Ping Zhang, Chun Meng,*
Xian-En Zhang,* and Qiangbin Wang*

As a typical protein nanostructure, virus-based nanoparticle (VNP) of simian virus 40 (SV40), which is composed of pentamers of the major capsid protein of SV40 (VP1), has been successfully employed in guiding the assembly of different nanoparticles (NPs) into predesigned nanostructures with considerable stability. However, the stabilization mechanism of SV40 VNP remains unclear. Here, the importance of inter-pentamer disulfide bonds between cysteines in the stabilization of quantum dot (QD)-containing VNPs (VNP-QDs) is comprehensively investigated by constructing a series of VP1 mutants of cysteine to serine. Although the presence of a QD core can greatly enhance the assembly and stability of SV40 VNPs, disulfide bonds are vital to stability of VNP-QDs. Cysteine at position 9 (C9) and C104 contribute most of the disulfide bonds and play essential roles in determining the stability of SV40 VNPs as templates to guide assembly of complex nanoarchitectures. These results provide insightful clues to understanding the robustness of SV40 VNPs in organizing suprastructure of inorganic NPs. It is expected that these findings will help guide the future design and construction of protein-based functional nanostructures.

Dr. F. Li,^[+] H. Chen,^[+] L. Ma, K. Zhou, Prof. Q. Wang
Suzhou Key Laboratory of Nanomedical Characterization
Division of Nanobiomedicine and i-Lab, Suzhou Institute of Nano-Tech and Nano-Bionics Chinese Academy of Sciences Suzhou, 215123, China
E-mail: qbwang2008@sinano.ac.cn
H. Chen, K. Zhou, Prof. C. Meng
College of Biological Science and Technology Fuzhou University Fuzhou, 350108, China
E-mail: mengchun@fzu.edu.cn
Z.-P. Zhang, Prof. X.-E. Zhang
State Key Laboratory of Virology Wuhan Institute of Virology Chinese Academy of Sciences Wuhan, 430071, China
E-mail: x.zhang@wh.iov.cn
^[+]These authors contributed equally to this work.

DOI: 10.1002/smll.201300860



1. Introduction

Protein nanostructures, such as fibers, rings, tubes, and cages, have attracted more and more attentions in the research of nano-bio interface as templates, containers, and carriers, due to well-defined structures, homogeneity, easy manipulation, and scaling-up preparation.^[1–7] As a typical group of protein nanostructures, virus-based nanoparticles (VNPs), which are generally cages or tubes formed by capsid proteins of viruses, have shown great promise for gene therapy vectors, nanoreactors, targeted drug delivery and templated assembly of complex nanostructures.^[8–12] For instance, the VNPs of cowpea chlorotic mottle virus have been used as a nanoreactor for single-enzyme catalysis studies;^[13] M13 phage has been employed to scaffold a light-harvesting antenna nanostructure for visible light-driven water oxidation.^[14] Recently, we have also explored the VNPs of simian virus 40 (SV40) to template the assembly of discrete, three-dimensional (3D), hybrid nanoarchitectures, in which a quantum dot (QD) is encapsulated at the center and a



Figure 1. Structure model of VP1 pentamer (PDB ID: 3bwg). The cysteines of a VP1 subunit (green) on the inter-pentamer interface are marked as red. Note that the C9 is not displayed in the model because it is located in the disordered N terminal arm which protrudes towards the lumen of capsid.

tunable number of gold nanoparticles (AuNPs) are positioned on the outer surface of VNPs,^[15,16] which holds great promise for building functional nanodevices. More recently, homogeneous AuNP clusters with a tunable core have been fabricated under the guidance of SV40 VNPs,^[17] which demonstrates the versatility of SV40 VNPs in scaffolding complex nanoarchitectures.

Structural stability is a key requirement for protein nanostructures acting as platforms of nanoscale manipulation, because it guarantees high yield of and precise dimensional control over the protein-guided assembly of nanoarchitectures. SV40 VNPs have proved to be robust and effective as a model nanoplatform. However, it is unclear how SV40 VNPs are stabilized during encapsulating or scaffolding inorganic nanoparticles (NPs). Understanding of the mechanism would benefit the rational design of VNP-based functional nanostructures and offer insightful instructions for control of interactions on nano-bio interface.

In natural SV40 virion, structure resolving^[18] as well as biochemical and virological analysis^[19–22] suggested that inter-pentamer disulfide bonds between cysteines of VP1 (the major capsid protein of SV40) may play important roles in the assembly and stabilization of SV40 capsid. Accordingly, disulfide bonding probably contributes to the stabilization of SV40 VNPs for templating the assembly of complex nanoarchitectures. However, the roles of VP1 cysteines in the templated assembly remain to be disclosed. One QD-containing SV40 VNP (VNP-QD) consists of 12 VP1 pentamers that arrange with a $T = 1$ icosahedral symmetry.^[15] Based on such a structural feature of VNPs and the structure of VP1 pentamer (**Figure 1**),^[23] cysteine at position 9 (C9), C49, C87, C104, C207 and C254 are distributed on the interface of neighboring pentamers in VNPs, in which C9 is positioned in the flexible N-terminal arm protruding into the inside of the protein cage, C49 is positioned in a beta sheet, and C87, C104, C207 and C254 are located in the BC loop, CD loop, EF loop and GH loop, respectively.^[18] Inter-pentamer C49-C49 disulfide bonds are unlikely to form because disulfide cross-linking occurs

Table 1. Definition of VP1 mutants.

Name of VP1 mutant	Cysteines mutated to serines	What to be examined
C9S	C9	The role of C9.
C87S	C87	The role of C87.
C104S	C104	The role of C104.
C207S	C207	The role of C207.
C254S	C254	The role of C254.
C9-104S	C9 and C104	The collective effect of C9 and C104, which were supposed to be essential for capsid assembly. ^[18]
C87-207S	C87 and C207	The role of the C87-C207 pair, which were supposed to be important for capsid assembly in living cells. ^[22]
C9-104-207S	C9, C104, and C207	The collective effect of C9, C104, and C207, which were supposed to be essential for capsid assembly. ^[18]
C87-104-207S	C87, C104, and C207	The collective effect of C104 and the C87-C207 pair.
C9-87-104-207S	C9, C87, C104, and C207	The collective effect of C9, C104, and the C87-C207 pair.

very rarely between parallel beta sheets.^[24,25] Therefore, we intend to examine how C9, C87, C104, C207 and C254 contribute to the robustness of SV40 VNPs when used as nanoscaffolds.

2. Results and Discussion

Mutation analysis was adopted to evaluate the importance of cysteines. To minimize the influence of mutation on protein configuration, cysteine was mutated to serine, because serine is the most analogous to cysteine. To quantitatively assess the importance of cysteines, a series of VP1 mutants were constructed (**Table 1**), including single mutants (C9S, C87S, C104S, C207S, and C254S), double mutants (C9-104S and C87-207S), triple mutants (C9-104-207S and C87-104-207S) and quadruple mutant (C9-87-104-207S). All coding sequences for mutant VP1s were verified by commercial sequencing to make sure successful abolishment of cysteines in VP1 proteins. According to the central dogma of molecular biology, information coded by DNA sequence is transferred to protein through transcription and translation with high fidelity. Therefore, the verified mutation of DNA sequence would lead to the successful replacement of cysteine by serine at predetermined sites. The mutants were expressed in *E. coli* efficiently and were successfully purified using a previous procedure for wild type VP1 (wtVP1).^[26] All the mutants could be purified to at least 85% purity using this procedure and kept the ability to form pentamers, the building blocks of SV40 VNPs (see supplementary results and Figure S1 in Supporting Information).

To examine the capability of VNPs formed from these mutants in templating complex nanoarchitectures, an

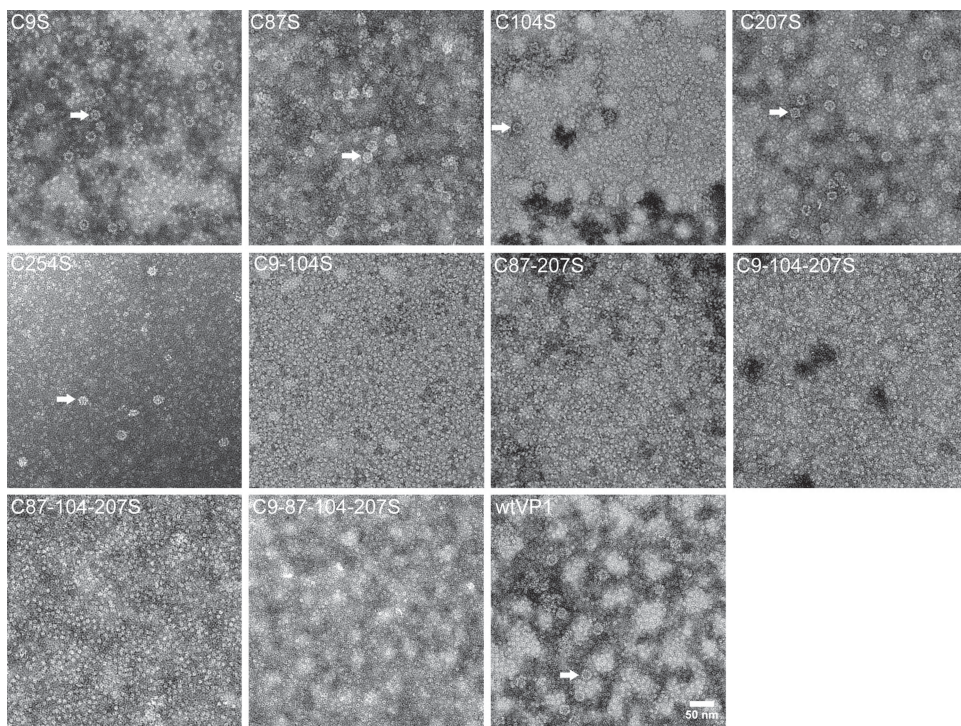


Figure 2. TEM images of self-assembly products of VP1s without any purification. All pictures were taken at the same magnification. White arrows point to representative VNP structures. Under our experimental conditions, all single mutants of VP1 formed VNPs like wtVP1. But few VNPs were observed in the self-assembly of all the multiple mutants, suggesting the significantly lowered self-assembly efficiency of VP1 by multiple abolishment of cysteines.

established method for assembling AuNP clusters with a QD core was used,^[17] which consists of two steps, I) encapsulating QDs inside VNPs via self-assembly, and II) binding of bis(p-sulfonatophenyl)-phenylphosphine (BSPP)-modified AuNPs (BSPP-AuNPs) onto the outside surface of VNPs.

Previous studies have suggested the important roles of cysteines in the assembly of SV40 VNPs or capsid.^[19–22] Our results of transmission electron microscopy (TEM) also showed that all multiple mutants presented worse capability in self-assembly into VNPs than wtVP1 (**Figure 2**). However, accompanying with the encapsulation of QDs coated with mercaptopropionic acid (MPA), assembly of all VP1 mutants into VNPs was significantly promoted. At a molar ratio of 12:1 (VP1 pentamers: QDs), all mutants formed VNP-QD hybrid NPs like wtVP1 (Figure S2). To quantify the co-assembly efficiencies of VP1 mutants with QDs, VNP-QDs and VP1 pentamers in the final products were collected through size exclusion chromatography (SEC), respectively. Then fractions of VNP-QDs and pentamers were analyzed using sodium dodecyl sulfate-polyacrylamide gel electrophoresis (SDS-PAGE)/densitometry (**Figure 3**), because it was unsuitable to determine protein content via absorption at 280 nm during SEC due to the strong absorption of QDs at this wavelength. The assembly efficiencies of all VP1s were consistently measured to be ~90%. All mutants present no significant difference from wtVP1 in encapsulating QDs (Figure 3). These results demonstrate that the QD core can promote the assembly of VP1 into VNPs and alleviate the influence of abolishing cysteines on the formation of VNPs.

Sucrose density gradient centrifugation (SDGC) is a well-established method for biomacromolecule analysis and purification. To further test the assembly of all mutated VP1s in the presence of QDs and to collect the assembled VNP-QDs, the co-assembly products were subjected to SDGC. The formation of sharp fluorescence bands after SDGC indicates efficient co-assembly of VP1 with QDs. The co-assembled products of VP1 mutants all exhibited the same pattern of QD fluorescence band in SDGC tubes as wtVP1 (Figure S3). This observation provides additional evidence that all mutants can co-assemble with QDs into VNP-QDs, similarly to wtVP1.

For each co-assembly product of VP1 mutant with QDs, the main band corresponding to VNP-QDs^[27] was harvested for stability examination. The samples were dialyzed to remove sucrose, concentrated by ultrafiltration, and observed under TEM. Unexpectedly, VNP-QDs of C9-104S, C9-104-207S, and C9-87-104-207S could not endure the purification process (SDGC-dialysis-concentration) and tended to dissociate because fewer VNPs and much more pentamers were observed in these samples than in VNP-QDs of wtVP1 (**Figure 4A** and Figure S4). In parallel, agarose gel electrophoresis was also run to characterize the purified VNP-QDs. As shown in Figure 4B, VNP-QDs of C9-104S, C9-104-207S, and C9-87-104-207S migrate slower than VNP-QDs of wtVP1 and their bands smear to some extent. In the smeared bands of these VNP-QDs, there is colocalization between QDs (fluorescence) and VP1 proteins (coomassie brilliant blue staining). The result suggests that structure changes

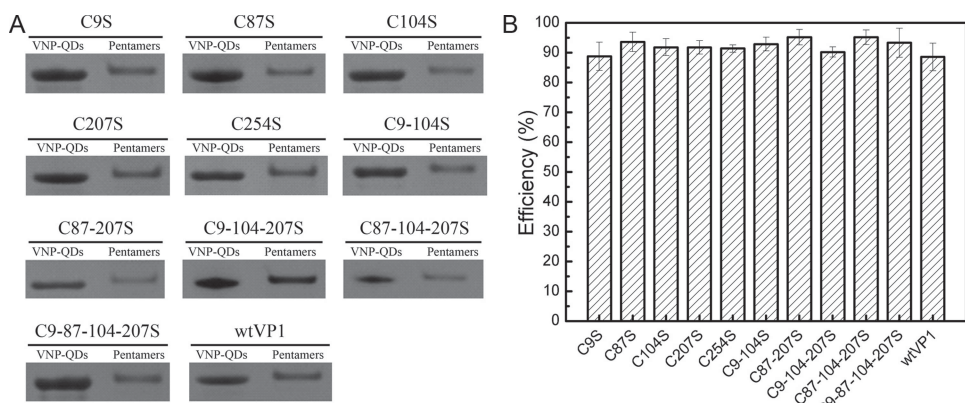


Figure 3. Analysis of VP1-QD co-assembly efficiencies. A) Representative images of SDS-PAGE of the two fractions corresponding to VNP-QDs and pentamers after separating the VP1-QD co-assembly products through SEC. All samples were concentrated to 0.2 mL after collection. For SDS-PAGE sampling, VNP-QD fractions were diluted eight times, while the pentamer fractions were not diluted. B) Quantification of VP1-QD co-assembly efficiencies using SDS-PAGE/densitometry. The assembly processes were carried out three times independently. Error bars represent standard deviations.

(partial dissociation) of VNP-QDs occurred, generating different species of VP1-QD complexes. However, no bands of free VP1 pentamers are seen, inconsistent with the TEM results. The disagreement might result from further dissociation of VP1-QD complexes of C9-104S, C9-104-207S, and C9-87-104-207S during TEM sampling and observation. Nevertheless, TEM and electrophoresis consistently show that VNP-QDs of all single mutants, C87-207S, and C87-104-207S are as stable as that of wtVP1 and that VNP-QDs of C9-104S,

C9-104-207S, and C9-87-104-207S are less stable. These results show that the C9-C104 pair is essential in stabilizing VNP-QDs. Meanwhile, C87 and C207 also contribute to the stabilization of VNP-QDs since VNP-QDs of the quadruple mutants presented the lowest stability (Figure 4).

To further assess the contribution of cysteines in stabilizing SV40 VNPs, mutated VNP-QDs are used as templates to assemble clusters of AuNPs. Excessive BSPP-AuNPs with a diameter of 4 nm are allowed to bind to VNP-QD

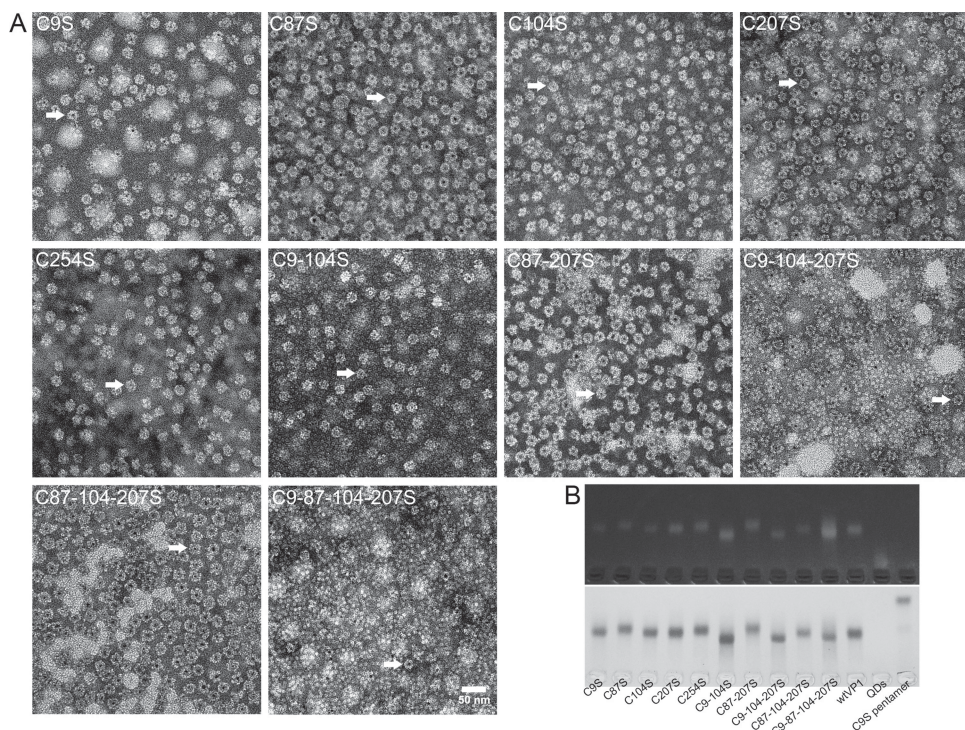


Figure 4. Characterization of purified VNP-QDs. A) TEM images of purified VNP-QDs formed from VP1 mutants. All pictures were taken at the same magnification. White arrows point to representative VNP-QDs structures. The visualization of QDs is sensitive to the extent of negative staining by phosphotungstic acid (PTA), because the CdSe@ZnS QDs have lower electron contrast than the PTA for protein visualization. Therefore, QDs are not always clearly distinguishable in the images. B) Agarose gel electrophoresis of VNP-QDs formed from VP1s as indicated, in comparison with QDs and C9S pentamers.

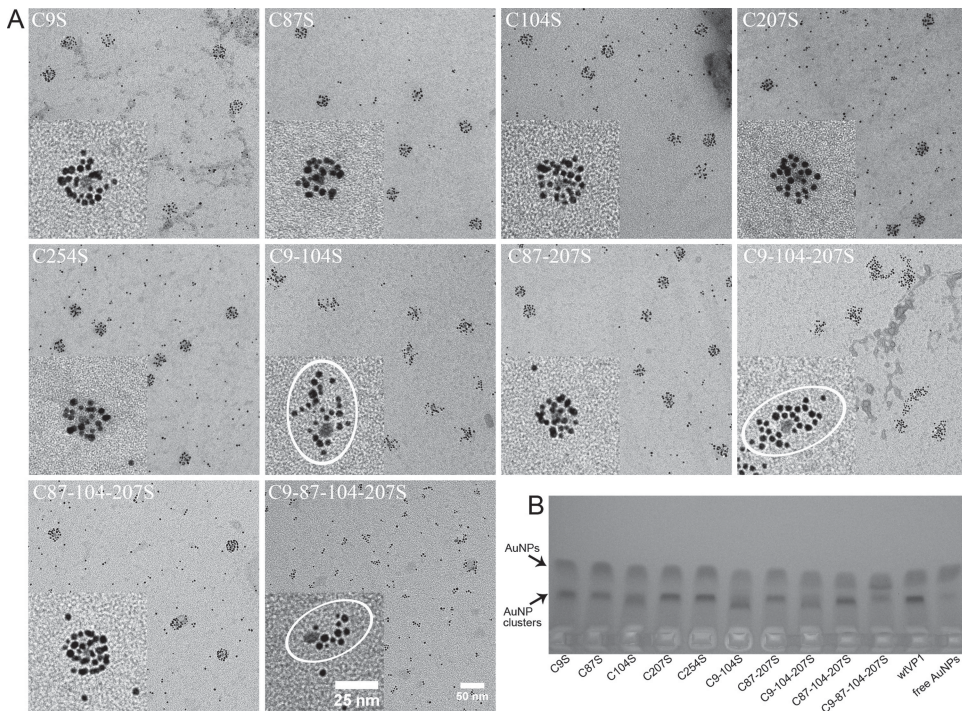


Figure 5. Characterization of AuNP assembly products templated by mutated VNP-QDs. A) TEM images of the assembly products. All pictures were taken at the same magnification. Insets are enlarged typical structures. The gray dots larger than AuNPs are QDs. C9S, C87S, C104S, C207S, C254S, C87-207S and C87-104-207S templated regular-shaped AuNP clusters as wtVP1 did (Figure S5), but C9-104S, C9-104-207S and C9-87-104-207S did not (marked with ellipses). Many free AuNPs were observed in the TEM images because excessive AuNPs were mixed with VNP-QDs for templated assembly to fully examine the influence of the negatively charged AuNPs on the structural stability of mutated VNP. B) Agarose gel electrophoresis of assembly products templated by VNP-QDs formed from VP1s as indicated, in comparison with free AuNPs.

surface through electrostatic interaction and amine-gold bonding as demonstrated recently.^[17] The assembly products are characterized by TEM and agarose gel electrophoresis. TEM observation showed that the assembly of AuNPs templated by C9S, C87S, C104S, C207S, C254S, C87-207S and C87-104-207S all generated round-shaped AuNP clusters with a uniform size of *ca.* 30 nm, at the center of which there was a QD (gray dot in the images). However, the VNPs composed of VP1 involved in mutation of both C9 and C104, including C9-104S, C9-87-104S and C9-87-104-207S, failed to template formation of the typical AuNP clusters. Instead, loosened or elongated structures of AuNP clusters were observed for C9-104S, C9-87-104S and only irregular aggregates of AuNPs and QDs were found for C9-87-104-207S (**Figure 5A** and Figure S5). Negative-staining TEM imaging of the irregular assembly products templated by C9-87-104-207S showed that the VNPs were dissociated and that AuNPs formed irregular complex with protein (Figure S6). The TEM results clearly show significant differences of AuNP assembly products templated by VNP-QDs of different VP1 mutants, pointing out the importance of the C9-C104 pair in stabilizing SV40 VNPs as templates for AuNP assembly. Electrophoresis also evidenced the difference of the three multiple mutants from other mutants as well as wtVP1 (Figure 5B). Due to excessive AuNPs were mixed with VNP-QDs for cluster formation, assembly products templated by wtVP1, single mutants, C87-207S and C87-104-207S resulted in two bands, one for AuNPs and the other for AuNP clusters (Figure 5B).

However, C9-104S and C9-87-104S resulted in a slower smeared band than the AuNP-clusters band of wtVP1, in agreement with that C9-104S and C9-87-104S merely guided the formation of irregular-shaped aggregates with larger sizes according to TEM observation. As for C9-87-104-207S, two faster bands appeared in contrast to the AuNP-clusters band, which is consistent with the formation of irregular AuNP-QD and AuNP-protein complexes with smaller sizes due to the dissociation of VNPs as indicated by TEM examination. These results corroborate the essential role of the C9-C104 pair in stabilizing QD-containing VNPs and in ensuring integrity of the templated AuNP nanoarchitectures. In addition, for the robustness of VNP nanotemplate, although the C87-C207 pair does not play the determinant role, they provide an additional stabilizing effect.

Finally, non-reducing SDS-PAGE was used to check the formation of disulfide bonds by the cysteines in VNP-QDs. SDG-purified VNP-QDs were first treated with loading buffer containing or not containing the reducing agent DL-Dithiothreitol (DTT) and were then subjected to SDS-PAGE. As shown in **Figure 6**, bands of VP1 monomer (molecular weight: *ca.* 42 kD) appeared in all lanes of VNP-QDs, no matter the samples were treated with DTT (DTT₊) or not (DTT₋). However, in DTT₋ lanes, smeared bands much larger than 42 kD were observed, indicating that disulfide bonds indeed formed in VNP-QDs. The smeared bands of VNP-QDs formed from C87S, C207S and C254S are similar to that of wtVP1, suggesting that C87, C207 and C254 contribute

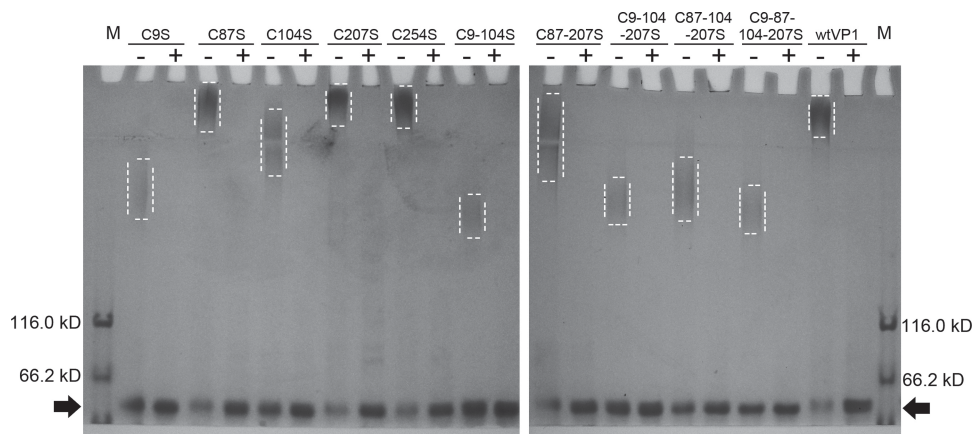


Figure 6. SDS-PAGE of purified VNP-QDs formed from VP1s as indicated. Samples were treated with loading buffer containing (+) or not containing (-) DTT before electrophoresis. Lanes M, protein molecular weight marker. The black arrows point to the band of VP1 subunit (monomer). The dotted rectangles indicate the smeared bands of VP1 multimers.

little to disulfide formation. However, the smeared bands of VNP-QDs formed from C9S, C104S and all multiple mutants ran faster than that of wtVP1, revealing that i) among the five cysteines, C9 and C104 play major roles in forming disulfide bonds; ii) the contributions of different cysteines are cumulative. The weakness of the smeared bands of VNP-QDs formed from C9-104S, C9-104-207S and C9-87-104-207S suggests that most disulfide bonds in wild type VNP-QDs are abolished in these mutated VNP-QDs, in agreement with their poor stability.

All the above findings provide insightful clues to the mechanism of the robustness of SV40 VNP in templating complex nanoarchitectures. Firstly, encapsulation of an inorganic core, independent of disulfide bonds, greatly promotes the assembly and stabilization of VNPs. Secondly, disulfide bonding by C9 and C104 provides further stabilization to VNPs. Thereby, a two-step mechanism is proposed for the assembly of VNPs of the SV40-related murine polyomavirus.^[28] In the first step, equilibrium between VNPs and pentamers is reached. In the second step, VNPs are fixed by the formation of disulfide bonds, which removes VNPs from the equilibrium reaction, resulting in efficient VNP assembly. Here in the co-assembly of QDs and SV40 VP1, QDs can provide additional driving force that shifts the equilibrium to the VNPs side, which is supported by the greatly enhanced assembly of all mutant VP1s by QDs. Referring to a model of viral coat protein assembly around preformed

inorganic cargos,^[29] QDs might promote the assembly of SV40 VNPs in two aspects as illustrated in **Figure 7**. One is that QDs might recruit VP1 pentamers and increase their local concentration through weak affinities between QD surface and some surface-exposed residues of VP1 such as histidine, tryptophan, methionine and cysteine.^[30] The other is that QDs might potentially act as scaffolds to favor the formation of correct inter-pentamer contacts including disulfide bonds as well as non-covalent bonds (hydrophobic interactions, salt bridges and hydrogen bonds),^[31] resulting in enhanced assembly and stability of VNPs.

SV40 has evolved to use cysteines/disulfide bonds as a mechanism for capsid stabilization.^[18] More interestingly, the virus smartly utilize the cellular factors to break the disulfide bonds for controlled release of genetic materials in specific subcellular compartments.^[32] Here, cysteines have been demonstrated to be involved in the stabilization of VNP-templated hybrid nanoarchitectures, opening up the possibility of designing novel intelligent nanocarriers for biosensing and delivery of bioactive molecules.

3. Conclusion

In conclusion, we have systematically studied the roles of inter-pentamer disulfide bonds in the assembly of complex nanoarchitectures templated by SV40 VNPs. Although a QD core can help assembly and stabilization of SV40 VNPs, disulfide bonds are found indispensable for VNP-QD stability. C9 and C104 contribute most of the disulfide bonds in VNP-QDs and play determinant roles in stabilizing VNP-QDs. Presence of either C9 or C104 is a prerequisite to guarantee the structural integrity of VNPs in templating assembly of complex nanoarchitectures. Our results highlight the importance of covalent linkage, such as disulfide bonds, to achieve robust protein/inorganic NP complexes, which have been demonstrated in our previous works.^[15–17]

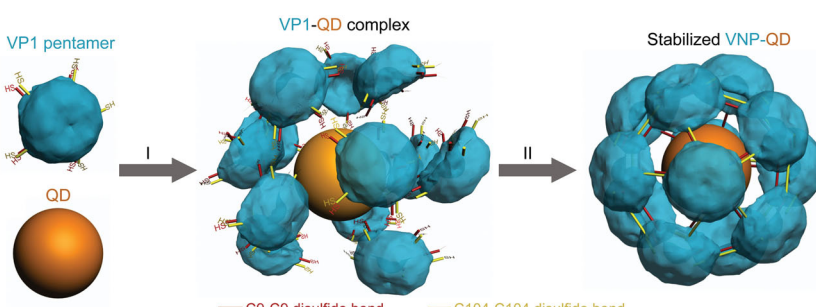


Figure 7. A proposed process of QD templated assembly of SV40 VNPs. I, recruitment of VP1 pentamers by QD; II, formation of inter-pentamers disulfide bonds and stabilization of VNP-QDs.

We expect that these findings will help guide the future design and construction of protein-based functional nanostructures.

4. Experimental Section

Mutagenesis of VP1: The mutagenesis of VP1 was achieved through standard PCR or overlap PCR. The gene of VP1 mutants were inserted into the pET32a(+) vector (Novagen) at *Nde*I-*Xba*I, resulting in pET32a-X (X represents the name of a VP1 mutant; see Table 1). The primers and templates for PCR are listed in Table S1. All the constructs were verified by sequencing (Sangon Biotech, Shanghai) and transformed into *E.coli* Rosetta (DE3) strain (Novagen). The proteins were expressed and purified using an ammonium sulfate precipitation/assembly/ultracentrifugation protocol, which was previously established.^[26] All VP1 proteins in the form of pentamers were stored in the dissociation buffer D (10 mM Tris-HCl, pH 8.8, 200 mM NaCl, 2 mM EDTA, 10 mM DTT and 5% glycerol).

Preparation of NPs: CdSe@ZnS QDs (emission peak: 620 nm) powder was purchased from Ocean NanoTech. Water solubilization with MPA and concentration determination were carried out as previously described.^[26] BSPP-AuNPs 4 nm in diameter was prepared according to a reported method.^[17]

Assembly of VNPs and VNP-QDs: For in vitro self-assembly, a VP1 protein solution (protein concentration: 0.25 mg/mL) was dialyzed against buffer A (10 mM Tris-HCl, pH 7.2, 1 mM CaCl₂, 0.5 M NaCl, and 5% glycerol) at 4 °C for 20 h with the buffer renewed at 10 h. For co-assembly of VP1 with QDs, one VNP for one QD was stoichiometrically preset. Because one VNP is composed of 12 VP1 pentamers,^[15] protein and QDs were mixed at a 12: 1 molar ratio of pentamers to QDs (protein concentration: 0.25 mg/mL) and the mixture were dialyzed against buffer B (10 mM Tris-HCl, pH 7.2, 1 mM CaCl₂, 250 mM NaCl, and 5% glycerol) at 4 °C for 20 h with the buffer renewed at 10 h.

Size Exclusion Chromatography: For analysis of co-assembly products of VP1 with QDs, a sample of 0.5 mL was applied to a Superdex 200 10/300 GL column on an AKTA prime plus FPLC system. Then the column was washed with buffer B at a flow rate of 0.5 ml/min. Fractions corresponding to VNPs and VP1 pentamers were collected respectively. Protein content in each fraction was analyzed using SDS-PAGE /densitometry.

Purification of VNP-QDs by SDGC: Co-assembly products of VP1 with QDs were loaded onto a 10%–50% sucrose density gradient and centrifuged at 38000 rpm (SW40 Ti rotor, Beckman) at 4 °C for 4 h. The SDGC tube was imaged using a digital camera with excitation by a portable UV lamp at 365 nm. The major fluorescence band was harvested, dialyzed against buffer B to eliminate sucrose and concentrated through ultrafiltration using an Amicon Ultra-15 Centrifugal Filter Unit with 100 kDa MW cut-off (Millipore).

Binding of AuNPs onto VNP-QD Outside Surface: BSPP-AuNPs were mixed with VNP-QDs in 0.02 M PB (pH 8) supplemented with 43 mM NaCl and 0.75 mM Tris, shaken at 260 rpm at room temperature overnight, and examined with TEM and agarose gel electrophoresis.

Agarose Gel Electrophoresis: VP1 pentamer or purified VNP-QD samples (20 μL) added with ficoll at a final concentration of 3% were loaded into 2% agarose gels in running buffer (40 mM Tris-HAc, pH 7.2). Electrophoresis was run for 40 min at 90 V with the gel tank in an ice bath. For the analysis of AuNP/VNP-QD complex, sam-

ples (20 μL) added with ficoll at a final concentration of 3% were loaded into 2% agarose gels in running buffer (44 mM Tris, 44 mM boric acid, 1 mM EDTA, pH 8.3). Electrophoresis was run for 20 min at 80 V at room temperature. Gels were imaged by a digital camera.

Transmission Electron Microscopy: For TEM imaging of self-assembled VNPs and co-assembled VNP-QDs, a diluted sample of 10 μL (VP1 protein concentration: 25 μg/mL) was applied to a carbon-coated copper grid, removed after 10 min with filter paper, and negatively stained for 3 min with 2% PTA. For TEM imaging of AuNP/VNP-QD complex, a sample of 10 μL was applied to a carbon-coated copper grid, blotted off after 10 min with filter paper, and unstained or negatively stained. All samples were imaged on an FEI Tecnai 20 TEM operated at 200 kV. Images were recorded with a Gatan UltraScan 894 CCD camera and processed with the ImageJ software.

Supporting Information

Supporting Information is available from the Wiley Online Library or from the author.

Acknowledgements

The authors thank the funding by CAS “Bairen Ji Hua” program and “Strategic Priority Research Program” (XDA01030200), MOST (2011CB965004), NSFC (31271076), NSF of Jiangsu Province (BK2012007), and CAS/SAFEA International Partnership Program for Creative Research Teams. The authors thank Mr. Lun Li for drawing the Scheme.

- [1] B. Worsdorfer, K. J. Woycechowsky, D. Hilvert, *Science* **2011**, *331*, 589.
- [2] J. C. Sinclair, K. M. Davies, C. Venien-Bryan, M. E. M. Noble, *Nat. Nanotechnol.* **2011**, *6*, 558.
- [3] A. P. Schoen, D. T. Schoen, K. N. L. Huggins, M. A. Arunagirinathan, S. C. Heilshorn, *J. Am. Chem. Soc.* **2011**, *133*, 18202.
- [4] M. Guli, E. M. Lambert, M. Li, S. Mann, *Angew. Chem. Int. Ed.* **2010**, *49*, 520.
- [5] P. Kaur, Y. Maeda, A. C. Mutter, T. Matsunaga, Y. J. Xu, H. Matsui, *Angew. Chem. Int. Ed.* **2010**, *49*, 8375.
- [6] S. Howorka, *Curr. Opin. Biotechnol.* **2011**, *22*, 485.
- [7] D. Men, Y. C. Guo, Z. P. Zhang, H. P. Wei, Y. F. Zhou, Z. Q. Cui, X. S. Liang, K. Li, Y. Leng, X. Y. You, X. E. Zhang, *Nano Lett.* **2009**, *9*, 2246.
- [8] L. S. Chen, M. Wang, W. C. Ou, C. Y. Fung, P. L. Chen, C. F. Chang, W. S. Huang, J. Y. Wang, P. Y. Lin, D. Chang, *Gene Ther.* **2010**, *17*, 1033.
- [9] S. J. Kaczmarczyk, K. Sitaraman, H. A. Young, S. H. Hughes, D. K. Chatterjee, *Proc. Natl. Acad. Sci. USA* **2011**, *108*, 16998.
- [10] G. J. Tong, S. C. Hsiao, Z. M. Carrico, M. B. Francis, *J. Am. Chem. Soc.* **2009**, *131*, 11174.
- [11] D. P. Patterson, P. E. Prevelige, T. Douglas, *Acs Nano* **2012**, *6*, 5000.
- [12] Y. J. Lee, H. Yi, W. J. Kim, K. Kang, D. S. Yun, M. S. Strano, G. Ceder, A. M. Belcher, *Science* **2009**, *324*, 1051.
- [13] M. Comellas-Aragones, H. Engelkamp, V. I. Claessen, N. A. J. M. Sommerdijk, A. E. Rowan, P. C. M. Christianen,

- J. C. Maan, B. J. M. Verduin, J. J. L. M. Cornelissen, R. J. M. Nolte, *Nat. Nanotechnol.* **2007**, *2*, 635.
- [14] Y. S. Nam, A. P. Magyar, D. Lee, J. W. Kim, D. S. Yun, H. Park, T. S. Pollock, D. A. Weitz, A. M. Belcher, *Nat. Nanotechnol.* **2010**, *5*, 340.
- [15] F. Li, D. Gao, X. M. Zhai, Y. H. Chen, T. Fu, D. M. Wu, Z. P. Zhang, X. E. Zhang, Q. B. Wang, *Angew. Chem. Int. Ed.* **2011**, *50*, 4202.
- [16] F. Li, Y. H. Chen, H. L. Chen, W. He, Z. P. Zhang, X. E. Zhang, Q. B. Wang, *J. Am. Chem. Soc.* **2011**, *133*, 20040.
- [17] F. Li, H. L. Chen, Y. J. Zhang, Z. Chen, Z.-P. Zhang, X.-E. Zhang, Q. B. Wang, *Small* **2012**, *8*, 3832.
- [18] R. C. Liddington, Y. Yan, J. Moulay, R. Sahli, T. L. Benjamin, S. C. Harrison, *Nature* **1991**, *354*, 278.
- [19] K. I. Ishizu, H. Watanabe, S. I. Han, S. N. Kanesashi, M. Hoque, H. Yajima, K. Kataoka, H. Handa, *J. Virol.* **2001**, *75*, 61.
- [20] C. C. Jao, M. K. Weidman, A. R. Perez, E. Gharakhanian, *J. Gen. Virol.* **1999**, *80*, 2481.
- [21] P. P. Li, A. Nakanishi, M. A. Tran, A. M. Salazar, R. C. Liddington, H. Kasamatsu, *J. Virol.* **2000**, *74*, 11388.
- [22] P. P. Li, A. Nakanishi, V. Fontanes, H. Kasamatsu, *J. Virol.* **2005**, *79*, 3859.
- [23] U. Neu, K. Woellner, G. Gauglitz, T. Stehle, *Proc. Natl. Acad. Sci. USA* **2008**, *105*, 5219.
- [24] B. Mao, *J. Am. Chem. Soc.* **1989**, *111*, 6132.
- [25] H. M. Fooks, A. C. R. Martin, D. N. Woolfson, R. B. Sessions, E. G. Hutchinson, *J. Mol. Biol.* **2006**, *356*, 32.
- [26] F. Li, K. Li, Z. Q. Cui, Z. P. Zhang, H. P. Wei, D. Gao, J. Y. Deng, X. E. Zhang, *Small* **2010**, *6*, 2301.
- [27] F. Li, Z. P. Zhang, J. Peng, Z. Q. Cui, D. W. Pang, K. Li, H. P. Wei, Y. F. Zhou, J. K. Wen, X. E. Zhang, *Small* **2009**, *5*, 718.
- [28] U. Schmidt, R. Rudolph, G. Bohm, *J. Virol.* **2000**, *74*, 1658.
- [29] I. Tsvetkova, C. Chen, S. Rana, C. C. Kao, V. M. Rotello, B. Dragnea, *Soft Matter* **2012**, *8*, 4571.
- [30] B. R. Peelle, E. M. Krauland, K. D. Wittrup, A. M. Belcher, *Langmuir* **2005**, *21*, 6929.
- [31] J. Nilsson, N. Miyazaki, L. Xing, B. Wu, L. Hammar, T. C. Li, N. Takeda, T. Miyamura, R. H. Cheng, *J. Virol.* **2005**, *79*, 5337.
- [32] D. Kuksin, L. C. Norkin, *J. Virol.* **2012**, *86*, 1555.

Received: March 18, 2013

Revised: July 28, 2013

Published online: